Journal of Applied Physics

Photoinduced heat conversion enhancement of metallic glass nanowire arrays

Cite as: J. Appl. Phys. **125**, 015102 (2019); https://doi.org/10.1063/1.5059423
Submitted: 20 September 2018 . Accepted: 10 December 2018 . Published Online: 27 December 2018

Ceren Uzun, Chandrasekhar Meduri, Niloofar Kahler, Luis Grave de Peralta, Jena M. McCollum, Michelle Pantoya, Golden Kumar, and Ayrton A. Bernussi

AIP Publishing

Journal of Applied Physics ARTICLE scitation.org/journal/jap

Photoinduced heat conversion enhancement of metallic glass nanowire arrays

Cite as: J. Appl. Phys. **125**, 015102 (2019); doi: 10.1063/1.5059423
Submitted: 20 September 2018 · Accepted: 10 December 2018 ·
Published Online: 27 December 2018

Ceren Uzun,[1,2] Chandrasekhar Meduri,[3] Niloofar Kahler,[3] Luis Grave de Peralta,[1,2] Jena M. McCollum,[4] Michelle Pantoya,[3] Golden Kumar,[3] and Ayrton A. Bernussi[2,5]

AFFILIATIONS

[1]Department of Physics and Astronomy, Texas Tech University, Lubbock, Texas 79409, USA
[2]Nanotech Center, Texas Tech University, Lubbock, Texas 79409, USA
[3]Department of Mechanical Engineering, Texas Tech University, Lubbock, Texas 79409, USA
[4]Department of Mechanical and Aerospace Engineering, University of Colorado Colorado Springs, Colorado Springs, Colorado 80918, USA
[5]Department of Electrical and Computer Engineering, Texas Tech University, Lubbock, Texas 79409, USA

ABSTRACT

Materials with high photo-thermal efficiency are essential in a wide variety of applications from medicine to renewable energy. Photo-thermal materials effectively absorb and convert light into heat. Nanostructures have proven to enhance absorption and heat retention owing to their large surface areas and restricted heat pathways. Here, we demonstrate that the optical absorption and heat conversion in near-infrared can be enhanced by using metallic glass nanowires whose geometry can be readily tailored through thermoplastic molding. Infrared thermography measurements and heat transport simulations reveal that the photoinduced temperature rise can be amplified by increasing the length of nanowires and decreasing the thickness of the supporting substrate. A temperature above 500 °C can be rapidly achieved to induce a controlled phase transformation from amorphous to crystalline state in metallic glass nanowires, while maintaining their geometrical integrity. Photoinduced temperature rise can be used in optical ignition applications as demonstrated by an example of thermite powder.

I. INTRODUCTION

High photo-thermal conversion efficiency is important in a number of applications including photo-thermal therapy, drug delivery, solar power collection, and thermoelectric conversion.[1–5] These applications typically involve highly absorbing nanostructured materials which effectively convert light into heat at desirable excitation wavelengths. Advances in fabrication of high aspect-ratio (length/diameter) nanowires and nanotubes have enabled the realization of artificial structures with unique thermal and optical properties.[6–8] Vertically aligned single-walled and multi-walled carbon nanotube (CNT) arrays have been extensively studied for photo-thermal-electric conversion applications due to their enhanced thermal conductivity,[9] light trapping efficiency,[10,11] and heat localization effects.[12] Photo-thermal energy conversion has also been demonstrated using semiconducting nanowire arrays (NWAs) of Si and GaAs.[13,14] High optical absorption and thermal conductivity of metallic (e.g., Bi and Cu) NWAs have been utilized for thermo-electric power generation applications.[15,16] Although different fabrication techniques such as electrospinning,[17] vapor-liquid-solid (VLS),[18] and catalytic growth[19] have been developed to synthesize nanowires of diverse materials, the inability to produce large NWAs and limited control over nanowire dimensions remain challenging. These manufacturing issues can be mitigated by using thermoplastic materials which can be directly embossed into nanostructures over wafer-scale areas. Polymeric materials are not suitable for photo-thermal applications because of poor optical absorption and low melting temperature. In contrast, metallic glasses (MGs) are ideal candidates for photo-thermal applications because of their metal-like optical and thermal properties and polymer-like shaping capability. Like thermoplastics, MGs can be molded into nanostructures above their glass transition temperature which is comparable

TABLE I. Labeling scheme and description of Pt-MG samples used in this study.

Label	Nanowire aspect-ratio, *l*/*d*	Substrate thickness, *t* (μm)	Description
F-t_1	...	50	Flat-thin
LAR-t_1	5	50	Low aspect ratio nanowires-thin
HAR-t_1	10	50	High aspect ratio nanowires-thin
F-t_2	...	100	Flat-thick
LAR-t_2	5	100	Low aspect ratio nanowires-thick
HAR-t_2	10	100	High aspect ratio nanowires-thick
VHR-t	>15	100	Very high aspect ratio nanowires

to plastics for some MGs.[20] The ability to easily reshape MGs into various profiles such as vertically aligned or bundled, smooth or rough, amorphous or crystalline, and convex or concave tip shaped nanowires is attractive for photo-thermal applications.[21,22] Previously, we showed that low optical reflectance (<2%) can be achieved at visible frequencies using MG NWAs.[23] Recently, we demonstrated a large photo-thermal heating response and strong heat localization effects using MG NWAs at moderate laser excitation powers.[24] However, quantitative correlation between the MG nanowire dimensions and photoinduced heating has not been established. In particular, theoretical analysis based on coupling of absorption, thermal conversion, and heat transport phenomena is required to understand the photo-thermal behavior of MG nanostructures. To achieve this, we combine simulations and direct temperature measurements in this study.

Here, we investigate the effects of MG nanowire characteristics such as the diameter, the length, and the effect of thickness of underlying substrate on the photo-thermal response in the near-infrared (NIR) region. Infrared (IR) thermography measurements revealed the significance of the substrate thickness and the nanowire aspect-ratio (length/diameter) in achieving high temperature during optical illumination. Temperature values measured using thermography of the photo-excited MG nanowires were verified by finite element simulations using COMSOL® Multiphysics software. Furthermore, we show that it is possible to induce a phase transformation in MG nanowires from amorphous to crystalline state and yet preserve their geometry. This allows the use of MG nanowires above the glass transition temperature as demonstrated by the ignition of thermite powder comprising aluminum (Al) and copper oxide (CuO) above 500 °C using Pt-based MG with a glass transition temperature of 230 °C.

II. SAMPLE FABRICATION

$Pt_{57.5}Cu_{14.7}Ni_{5.3}P_{22.5}$ metallic glass (Pt-MG) was prepared by water quenching and thermoplastically patterned using nanoporous alumina templates. Details about the synthesis and the patterning of Pt-MG have been reported elsewhere.[23] Unpatterned and nanopatterned Pt-MG discs of about 8 mm diameter and different thicknesses were fabricated. All nanopatterned samples consisted of vertical nanowires with diameter $d \sim 100$ nm, arranged in a nearly hexagonal lattice with period $p \sim 250$ nm, and attached to the Pt-MG substrate. Nanowires of other diameters were also studied, but for the purpose of theoretical analysis, we focus only on 100 nm diameter NWs. The length (l) of nanowires and the thickness (t) of supporting substrate were independently varied to study their effects on photoinduced heating. For convenience, a sample labeling scheme (Table I) is used based on the surface pattern (nanowires) and the substrate thickness. In order to demonstrate the effects of topography and substrate thickness on the photoinduced temperature rise, the samples with nanowires of varying aspect-ratios and two substrate thicknesses (see Table I) were investigated.

Figure 1 shows the schematic and two representative scanning electron microscopy (SEM) images of samples with low and high aspect-ratio nanowires. There is a ±20 nm variation in diameter of nanowires due to pore size distribution in alumina templates. In addition to the amorphous control samples F-t_1, LAR-t_1, HAR-t_1, F-t_2, LAR-t_2, and HAR-t_2, two Pt-MG discs with very long nanowires ($l/d > 15$) in amorphous and crystalline states (VHR-t) were prepared to analyze the effect of photoinduced heating on the phase transformation (crystallization, melting, and ignition).

III. RESULTS AND DISCUSSION

The photoinduced temperature rise on nanopatterned and flat MG surfaces strongly depends on the absorption (A), heat localization, and thermal conductivity of nanowires and

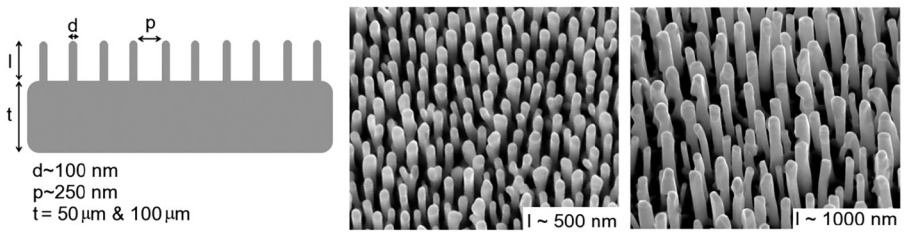

FIG. 1. Schematic illustration of sample geometry (not to scale) and SEM images of two Pt-MG samples patterned with nanowires of different lengths.

the substrate.[24] In order to determine the absorption characteristics of patterned MGs, we measured their integrated diffuse reflectance (R) at different incident angles (θ_i) at $\lambda = 980$ nm wavelength using the procedures described in our previous work.[23] In short, samples were mounted over a holder that was attached to a computer-controlled rotation stage at the center of an integrating sphere. Samples were illuminated by a continuous-wave laser emitting at $\lambda = 980$ nm, and the intensity of the scattered light was measured by a calibrated photodetector that was placed in one of the ports of the integrating sphere. Figure 2 shows measured angular dependence of absorption ($A = 1 - R$) for both nanopatterned (HAR-t_1, LAR-t_1, HAR-t_2, and LAR-t_2) and flat (F-t_1 and F-t_2) samples. Absorption as high as ~94.5% over a wide range of incident angles (for $|\theta_i| < 30°$) was determined for patterned samples with high aspect-ratio nanowires ($l/d \sim 10$). The absorption decreases to ~84.5% and ~50% for lower aspect-ratio ($l/d \sim 5$) nanowire and flat samples, respectively. The large absorption observed for high aspect-ratio nanowires is attributed to the efficient light trapping mechanism due to multiple reflections of incident light.[23] As expected, changes in the substrate thickness do not play any significant role in the optical absorption of the investigated samples. The observed peaks in the absorption near $\theta_i = 0°$ (especially for samples F-t_1 and F-t_2) are experimental artifacts arising from the loss of scattered light back to the incident port aperture of the integrating sphere as a result of the specular reflection from the samples.

The photoinduced temperature rise on the surface of patterned and flat MG samples was determined using the IR thermography setup described in our previous work.[24] Briefly, it consists of a continuous wave $\lambda = 980$ nm semiconductor laser diode, collimating and focusing lenses, and a 480 × 640-pixel resolution thermal camera. The edges of the MG sample were attached to two glass strips (~250 μm thick) forming a rectangular channel on a solid aluminum block holder. As a result, both the top and the bottom of the MG samples were exposed to air during the measurements, minimizing the heat loss due to the aluminum holder. The samples were illuminated by a laser with a ~350 μm diameter spot-size. The maximum temperatures of the illuminated areas were determined for laser power densities varying from 0.5 to 11.5 W/mm^2 using the thermal camera. All data acquisitions were performed at ~30 s after thermal equilibrium was reached on the sample surface. In this section, we focus on temperature rise up to the glass transition temperature (T_g) of Pt-MG (~230 °C)[21,25] to avoid potential changes in shape and structural state due to crystallization.

Representative thermal images of a nanopatterned (HAR-t_1) and a flat (F-t_1) Pt-MG sample of the same thickness obtained at an incident laser power density of ~2.8 W/mm^2 are shown in Figs. 3(a) and 3(b), respectively. Strong heat localization at the illuminated area with a maximum temperature rise of about 185 °C was determined for the nanopatterned sample [Fig. 3(a)]. The heat localization is due to significantly lower heat flow in the lateral direction in nanowires due to boundary scattering.[26] In contrast, a diffuse hot spot is observed for the flat sample [Fig. 3(b)] and the maximum temperature rise from the room temperature was merely $\Delta T \sim 90$ °C. Lower temperature rise on the flat sample is a combined effect of less optical absorption and higher lateral heat loss in the substrate.

Figure 4 shows the maximum temperature values achieved for nanopatterned (HAR-t_1, LAR-t_1, HAR-t_2, and LAR-t_2) and flat (F-t_1 and F-t_2) MG samples illuminated at increasing laser power densities. Photoinduced temperature rise measurements revealed a strong thickness dependence in flat and patterned MGs. For flat samples, the maximum temperatures were measured as ~138 °C and ~197 °C for thicknesses of 100 μm and 50 μm, respectively (at 6.2 W/mm^2). This is attributed to changes in the thermal resistance with the substrate thickness. A longer conduction path in the thicker substrate results in higher heat loss, and, therefore, lower equilibrium temperature. Similar but less pronounced effect of substrate thickness is observed in the nanopatterned samples (Fig. 4).

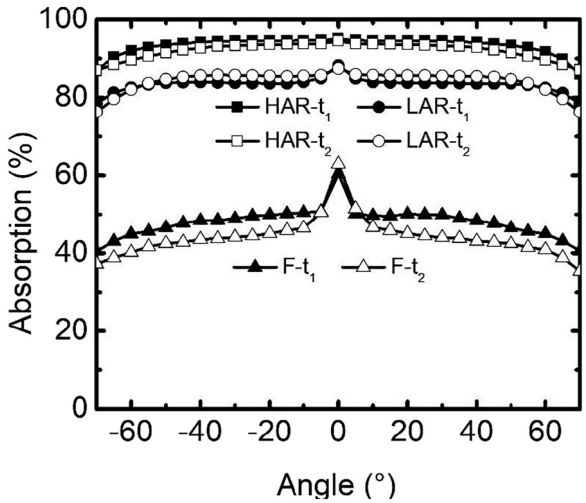

FIG. 2. Measured absorption angular dependence of patterned (HAR-t_1, LAR-t_1, HAR-t_2, and LAR-t_2) and flat (F-t_1 and F-t_2) Pt-MG samples at $\lambda = 980$ nm.

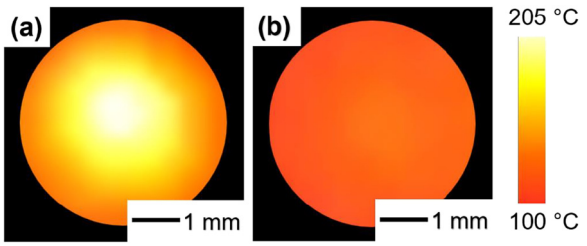

FIG. 3. Thermal images of (a) HAR-t_1 and (b) F-t_1 Pt-MG samples obtained at an identical laser power density of ~2.8 W/mm^2.

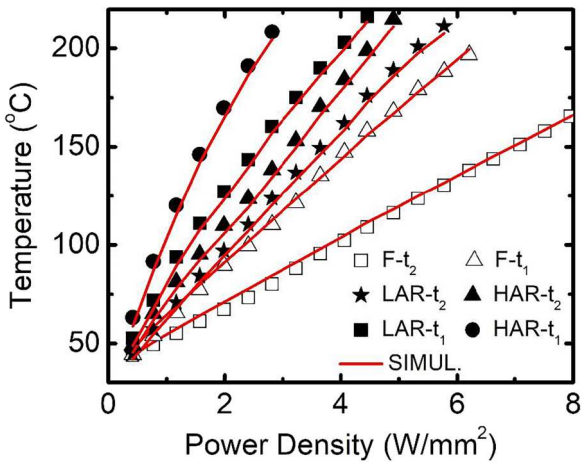

FIG. 4. Measured and simulated maximum photoinduced temperature rise for patterned (HAR-t_1, LAR-t_1, HAR-t_2, and LAR-t_2) and unpatterned (F-t_1 and F-t_2) Pt-MG samples at different laser excitation power densities.

This is because the heat transport in the nanopatterned samples is predominantly governed by the conduction through nanowires. Although the samples with similar aspect-ratio nanowires exhibit comparable absorption (see Fig. 2), the thinner specimens heat to higher temperatures (Fig. 4). About 52% increase in temperature at 2.8 W/mm^2 was measured when the substrate thickness was decreased by half for high aspect-ratio (~10) nanowires. A similar trend was observed for the low aspect-ratio nanowires but with only 31% increase in temperature for the thinner substrate. The difference in maximum temperature in thin and thick samples grows with increasing incident laser power density (Fig. 4). Heat conversion is the limiting factor at low laser power density, whereas the thermal losses control the temperature at high laser power density.

Thermal measurements on the MG samples with similar thickness revealed the importance of surface texture in achieving high photoinduced heat generation. The nanopatterned samples of any thickness generate significantly higher temperatures than the flat counterparts. At an incident laser flux of 4.9 W/mm^2, the thick patterned samples reach 60% and 82% higher temperatures with nanowires of aspect-ratios of 5 (LAR-t_2) and 10 (HAR-t_2), respectively. Similarly, about 40% (86%) increase in photoinduced temperature was observed with nanowires in thin samples LAR-t_1 (HAR-t_1) at 2.8 W/mm^2. As shown in Fig. 4, due to combined effects of surface patterning and substrate thickness, maximum temperature as high as 205 °C can be achieved in Pt-MG under a moderate laser excitation power of ~2.8 W/mm^2. The flat samples require significantly higher laser power density to reach comparable temperatures because of weak absorption. The effective thermal conductivity of nanopatterned samples (nanowires + substrate) is expected to be lower than the flat samples because of enhanced boundary scattering in nanowires. This attribute, combined with the large absorption of nanowires, results in a significant temperature rise in nanopatterned MGs. Therefore, despite the thermal loss through the thick metallic substrate, the amount of heat converted is significantly larger than the heat dissipated by the sample and the temperature rises rapidly as the incident laser power is increased.

To further understand the photo-thermal behavior of MGs, we performed numerical simulations using COMSOL Multiphysics software with Heat Transfer in Solids module. Vertically aligned cylindrical nanowires with dimensions approximated from the SEM images were used in simulations to mimic the experimental conditions. A unit cell structure comprising a Pt-MG nanowire embedded in air was placed over a thick square Pt-MG substrate [Fig. 5(a)]. Appropriate periodic boundary conditions were used in all simulations to emulate the periodic NWAs in experimental samples. A two-dimensional Gaussian heat source profile was used to mimic the laser heating on the top of patterned (and flat) surfaces. Convective heat flux was also taken into consideration due to the presence of air between the nanowires. The emissivity used in the simulations was obtained by normalizing the absorption values to unity from the measured integrated diffuse reflectance of our samples (see Fig. 2). In our simulations, we used the MG thermal conductivity of 10 W/m K.[25] Representative simulated temperature distributions on the top and the bottom of a single nanowire unit cell with $l/d = 10$ and $t = 50\,\mu$m (HAR-t_1) at a power density of ~2.8 W/mm^2 are shown in Figs. 5(b) and 5(c), respectively. Most of the heat is transferred from the top to the bottom of the nanowire due to a large thermal conductivity of MG with a corresponding temperature drop of ~10%. Simulated temperature curves for nanopatterned (HAR-t_1, LAR-t_1, HAR-t_2, and LAR-t_2) and flat (F-t_1 and F-t_2) MG samples at different laser power densities are also shown in Fig. 4 for comparison with experimental data. A good agreement between the simulations and the

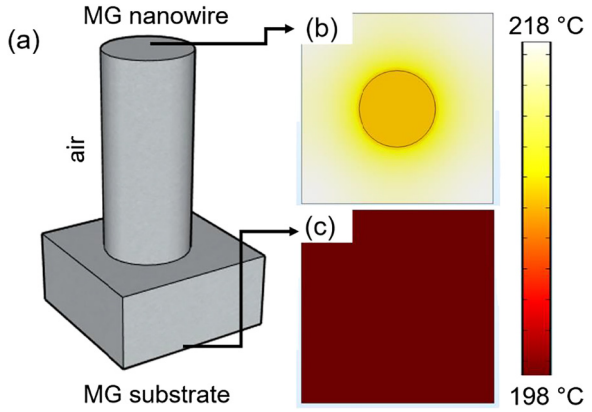

FIG. 5. (a) Schematic illustration of single nanowire unit cell geometry (not to scale) used in the simulations. Simulated temperature distribution of a single nanowire unit cell with $l/d = 10$ and $t = 50\,\mu$m (HAR-t_1) at a power density of ~2.8 W/mm^2 (b) from the top view and (c) from the bottom view.

experiments is evident for flat and patterned samples. This indicates that the numerical analysis can be used to adequately describe the heat transport in patterned MGs and also to predict the optimal texture and substrate thickness required for maximum temperature in photo-thermal heating.

In order to investigate the effects of the atomic structure on photo-thermal heating of nanopatterned MGs, we fabricated amorphous and crystalline Pt-MG samples comprising nanowires with a similar aspect ratio $l/d > 10$. Laser heating experiments with power densities up to 11.5 W/mm^2 were performed to exceed the crystallization temperature of Pt-MG.[25] Figure 6(a) shows the maximum photoinduced temperature rise on the surface of the amorphous and the crystalline (VHR-t) samples for different laser power densities. The maximum temperature on the crystalline sample continuously rises with increasing laser power density reaching a temperature of ~557 °C at 9.1 W/mm^2. In contrast, the amorphous sample exhibits a step-like jump in temperature above 300 °C. The temperature jump originates from the amorphous to crystalline phase transition in Pt-MG.[21,25] To verify this, we performed a second set of temperature measurements on the amorphous sample at the same spot after reaching 550 °C during the first experiment. As clearly shown in Fig. 6(a) (Exp#2), the temperature jump was no longer observed. Amorphous to crystalline transformation (devitrification) is irreversible, and, therefore, the second heating curve appears smooth alike the curve for the crystalline sample. Two heating curves measured at the same spot confirm that the step change in temperature in amorphous nanopatterned Pt-MG is due to photo-thermal heating induced crystallization. The crystalline state of Pt-MG has different optical (refractive index) and thermal (conductivity) properties than the amorphous state. Consequently, the first (Exp#1) and the second (Exp#2) photo-thermal temperature curves are different. The temperature curves of two crystalline samples, i.e., the as-prepared (VHR-t Crystalline) and the crystallized by laser heating (VHR-t Amorphous Exp#2) also differ due to a slight change in geometry of nanowires upon laser exposure. The as-prepared sample was crystallized during thermoplastic molding where the nanowires were confined in the alumina template. Therefore, the nanowire shape and size remained intact during crystallization [Fig. 6(b)]. The laser-induced heating results in slight distortion of MG nanowires above T_g due to the action of capillary stress on an unconfined state [Fig. 6(c)].[27] The morphological disparity between two crystalline samples affects their optical absorption and thermal transport, which result in a different photo-thermal response. It is also worth noting that the as-prepared crystalline nanopatterned sample generates significantly higher heating than the amorphous counterpart exposed to the same laser flux [Fig. 6(a)]. Therefore, crystallized MG nanowires are ideally suited for high temperature photo-thermal applications.

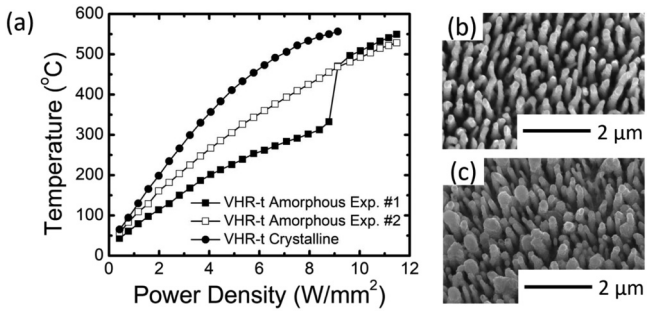

FIG. 6. (a) Measured maximum photoinduced temperature rise on patterned amorphous and crystalline Pt-MG (VHR-t) samples at different laser excitation power densities. SEM image of (b) the as-prepared crystalline sample (VHR-t Crystalline) and (c) the sample crystallized by photoinduced heating (VHR-t Amorphous Exp #2).

An important photo-thermal application is laser induced ignition of a thermite reaction. Thermite is a mixture of metal fuel and metal oxide particles that undergo an exothermic reaction upon heating to ignition. Large heat released in thermite reaction is utilized in a wide range of applications in defense, manufacturing, and metallurgy.[28,29] The amount of released heat and the ignition temperature depend on the composition and the size of the thermite particles.[30] Various techniques such as flash,[31] electrical,[32] mechanical,[33] and laser stimuli[34] have been used to stimulate thermite ignition. Laser ignition has gained significant interest because of safety, insensitivity to environmental conditions, remotely accessible, nonintrusive, and contactless heating of thermites.[35] However, high power lasers such as CO_2, excimer, or Nd:YAG are required[35] to attain ignition temperatures due to poor absorption of metal particles except at the plasmon resonance. Crystallized MG nanowires are good candidates for laser ignition of thermite powders due to their ability to generate high temperatures at moderate incident laser powers, therefore enabling the use of more compact and low-cost semiconductor diode lasers for ignition. To this end, we experimented with a thermite mixture of stoichiometrically balanced nano-sized Al (~100 nm) and CuO (~25-50 nm) powders that ignite at 550 °C with an exothermic heat of 4.1 kJ/g.[36] A homogeneous mixture was prepared by suspending the powders in isopropyl alcohol carrier fluid followed by sonication for 1 h. The sonication process breaks up agglomerates and provides more homogeneous mixing between fuel and oxidizer powders. The solution was spin coated on crystalline Pt-MG nanowires and dried in air to form a conformal thermite layer. Three coats were applied to achieve a semi-continuous thermite layer necessary for propagation of the reaction front upon ignition. As shown in Fig. 7(a), some sections of the MG nanowires were not covered with thermite to allow absorption of laser by the nanowires. The same continuous wave NIR semiconductor laser diode ($\lambda = 980$ nm) employed in the thermography experiments, but with a reduced spot size (spot size diameter 50-70 μm), was used for the ignition tests [Fig. 7(b)]. The thermite powder coated on a glass slide was also exposed to the same laser conditions for comparison. The thermite powder coated onto MG NWAs ignited at ~12 W/mm^2 power density and the ignition resulted

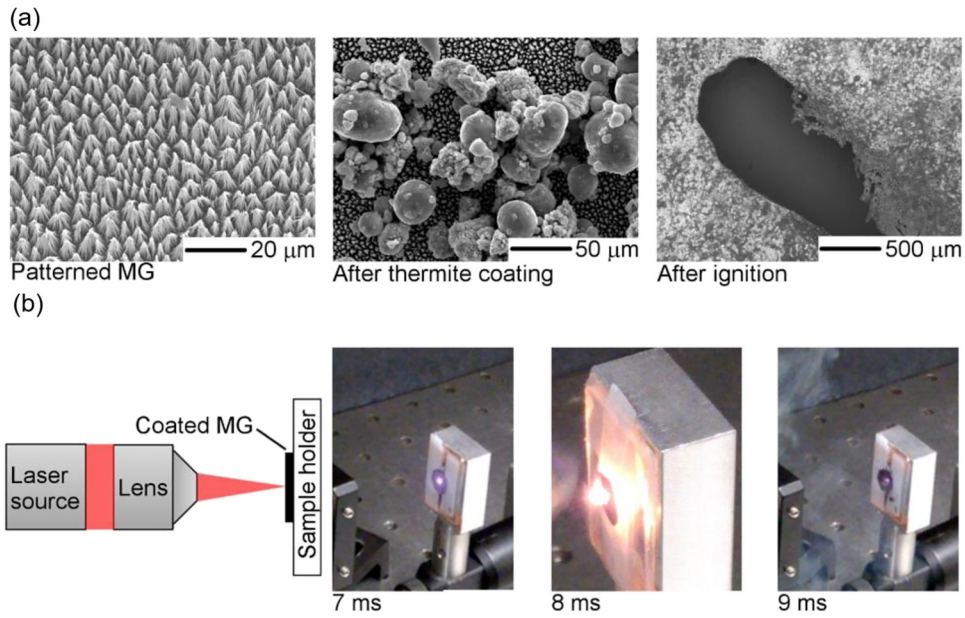

FIG. 7. (a) SEM images of nano-patterned Pt-MG in the as-prepared state, after coating with thermite mixture, and after laser ignition of thermite. (b) Schematic illustration of laser ignition setup and still images captured at different times from the video recording obtained with a laser power density of ~12 W/mm^2.

in the formation of a hole in the MG NWA sample due to a large exothermic heat generated during the ignition process [Fig. 7(a)]. As shown by the still images [Fig. 7(b)] captured from the video streaming using a CCD camera, the ignition started at about 8 ms after laser exposure. The reaction products that were reclaimed, analyzed using energy-dispersive X-ray (EDX), and composed of aluminum oxide (Al_2O_3) and copper (Cu) were consistent with the balanced chemical reaction:

$$2Al + 3CuO \rightarrow Al_2O_3 + 3Cu.$$

In contrast, the ignition was not observed for the thermite mixture on the glass slide, even up to an order of magnitude higher than laser power densities. Non-ignition is attributed to the significantly less absorption and lower temperature of the unpatterned substrate that did not provide sufficient thermal stimuli to ignite the thermite powder compared to the crystallized MG nanowires (i.e., ~95% laser power absorption) in the NIR. In addition to the large absorption, the MG nanowire architecture results in fast temperature rise due to minimal thermal losses through lateral heat conduction (see Fig. 5). Thus, the ignition temperature of the thermite can be reached at lower incident laser powers using MG NWA, eliminating the need for bulky and costly high-power lasers typically used for ignition.

IV. CONCLUSIONS

In this study, we investigated the influence of surface texture, substrate thickness, and structural state of MG samples for achieving high temperatures upon NIR laser illumination. IR thermography measurements show that high photo-thermal temperatures can be achieved by reducing the substrate thickness and by increasing the length of surface nanowires. The effect of thickness is attributed to change in the thermal resistance of MG substrate. Longer nanowires generate higher temperature as a result of enhanced optical absorption and confinement of heat in nanoscale channels. Experimental results were verified by the finite element analysis of the heat transport, which can be used for the optimization of surface texture for a desirable photo-thermal outcome. We further showed that the phase transformation of MG nanowires from amorphous to crystalline state can be induced by optical heating. The crystallized nanowires exhibit superior photo-thermal response compared to the glassy ones. Therefore, the phase change in MG nanowires is not a limiting factor for photo-thermal applications. Our results suggest that MG nanowires can be utilized in photo-thermal applications due to their high absorption and heat transfer capabilities. We demonstrate one such application where a thermite mixture was ignited at significantly lower laser flux using MG nanowires than the bare sample.

ACKNOWLEDGMENTS

G.K. and C.M. acknowledge support from the National Science Foundation (NSF) (Nos. CMMI-1663568 and NSF-CAREER-1653938). M.P. is thankful for the support from the Army Research Office (ARO) (Grant No. W911NF-17-1-0387)

and the Office of Naval Research (ONR) (Grant No. N00014-16-1-2079).

REFERENCES

[1]X. H. Huang, I. H. El-Sayed, W. Qian, and M. A. El-Sayed, "Cancer cell imaging and photothermal therapy in the near-infrared region by using gold nanorods," J. Am. Chem. Soc. **128**, 2115–2120 (2006).
[2]S. R. Sershen, S. L. Westcott, N. J. Halas, and J. L. West, "Temperature-sensitive polymer—nanoshell composites for photothermally modulated drug delivery," J. Biomed. Mater. Res. **51**, 293–298 (2000).
[3]H. Ghasemi, G. Ni, A. M. Marconnet, J. Loomis, S. Yerci, N. Miljkovic, and G. Chen, "Solar steam generation by heat localization," Nat. Commun. **5**, 4449 (2014).
[4]E. Sani, S. Barison, C. Pagura, L. Mercatelli, P. Sansoni, D. Fontani, D. Jafrancesco, and F. Francini, "Carbon nanohorns-based nanofluids as direct sunlight absorbers," Opt. Express **18**, 5179 (2010).
[5]L. L. Baranowski, G. J. Snyder, and E. S. Toberer, "Concentrated solar thermoelectric generators," Energy Environ. Sci. **5**, 9055 (2012).
[6]R. Yang, G. Chen, and M. S. Dresselhaus, "Thermal conductivity of simple and tubular nanowire composites in the longitudinal direction," Phys. Rev. B **72**, 1–7 (2005).
[7]D. G. Cahill, W. K. Ford, K. E. Goodson, G. D. Mahan, A. Majumdar, H. J. Maris, R. Merlin, and S. R. Phillpot, "Nanoscale thermal transport," J. Appl. Phys. **93**, 793 (2003).
[8]Y. J. Lee, D. S. Ruby, D. W. Peters, B. B. McKenzie, and J. W. P. Hsu, "ZnO nanostructures as efficient antireflection layers in solar cells," Nano Lett. **8**, 1501–1505 (2008).
[9]R. H. Baughman, A. A. Zakhidov, and W. A. De Heer, "Carbon nanotubes—The route toward applications," Science **297**, 787–792 (2002).
[10]K. Mizuno, J. Ishii, H. Kishida, Y. Hayamizu, S. Yasuda, D. N. Futaba, M. Yumura, and K. Hata, "A black body absorber from vertically aligned single-walled carbon nanotubes," Proc. Natl. Acad. Sci. U. S. A. **106**, 6044–6047 (2009).
[11]Z. P. Yang, L. Ci, J. A. Bur, S. Y. Lin, and P. M. Ajayan, "Experimental observation of an extremely dark material made by a low-density nanotube array," Nano Lett. **8**, 446–451 (2008).
[12]P. Yaghoobi, V. M. Moghaddam, and A. Nojeh, "Heat trap: Light-induced localized heating and thermionic electron emission from carbon nanotube arrays," Solid State Commun. **151**, 1105–1108 (2011).
[13]P. B. Roder, B. E. Smith, E. J. Davis, and P. J. Pauzauskie, "Photothermal heating of nanowires," J. Phys. Chem. C **118**, 1407–1416 (2014).
[14]J. Walia, N. Dhindsa, J. Flannery, I. Khodabad, J. Forrest, R. Lapierre, and S. S. Saini, "Enhanced photothermal conversion in vertically oriented gallium arsenide nanowire arrays," Nano Lett. **14**, 5820–5826 (2014).
[15]M. S. Dresselhaus, X. Sun, Z. Zhang, S. B. Cronin, T. Koga, J. Y. Ying, and G. Chen, "The promise of low-dimensional thermoelectric materials," Microscale Thermophys. Eng. **3**, 89–100 (1999).
[16]M. T. Barako, S. Roy-Panzer, T. S. English, T. Kodama, M. Asheghi, T. W. Kenny, and K. E. Goodson, "Thermal conduction in vertically aligned copper nanowire arrays and composites," ACS Appl. Mater. Interfaces **7**, 19251–19259 (2015).
[17]S. M. Choi, J. H. Kim, J. Y. Jung, E. Y. Yoon, and W. B. Kim, "Pt nanowires prepared via a polymer template method: Its promise toward high Pt-loaded electrocatalysts for methanol oxidation," Electrochim. Acta **53**, 5804–5811 (2008).
[18]A. S. Paulo, J. Bokor, R. T. Howe, R. He, P. Yang, D. Gao, C. Carraro, and R. Maboudian, "Mechanical elasticity of single and double clamped silicon nanobeams fabricated by the vapor-liquid-solid method," Appl. Phys. Lett. **87**, 053111 (2005).
[19]A. W. Z. Li, S. S. Xie, L. X. Qian, B. H. Chang, B. S. Zou, W. Y. Zhou, R. A. Zhao, and G. Wang, "Large-scale synthesis of aligned carbon nanotubes," Am. Assoc. Adv. Sci. **274**, 1701–1703 (2016).
[20]G. Kumar, H. X. Tang, and J. Schroers, "Nanomoulding with amorphous metals," Nature **457**, 868–872 (2009).
[21]G. Kumar, A. Desai, and J. Schroers, "Bulk metallic glass: The smaller the better," Adv. Mater. **23**, 461–476 (2011).
[22]J. Schroers, G. Kumar, T. M. Hodges, S. Chan, and T. R. Kyriakides, "Bulk metallic glasses for biomedical applications," JOM **61**, 21–29 (2009).
[23]H. J. Tarigan, N. Kahler, N. S. Ramos, G. Kumar, and A. A. Bernussi, "Low reflectance of nano-patterned Pt-Cu-Ni-P bulk metallic glass," Appl. Phys. Lett. **107**, 021903 (2015).
[24]C. Uzun, N. Kahler, L. G. De Peralta, G. Kumar, and A. A. Bernussi, "Photo-induced-heat localization on nanostructured metallic glasses," J. Appl. Phys. **122**, 1–6 (2017).
[25]J. Schroers and W. L. Johnson, "Highly processable bulk metallic glass-forming alloys in the Pt-Co-Ni-Cu-P system," Appl. Phys. Lett. **84**, 3666–3668 (2004).
[26]Z. Cheng, L. Liu, S. Xu, M. Lu, and X. Wang, "Temperature dependence of electrical and thermal conduction in single silver nanowire," Sci. Rep. **5**, 10718 (2015).
[27]G. Kumar and J. Schroers, "Write and erase mechanisms for bulk metallic glass," Appl. Phys. Lett. **92**, 90–93 (2008).
[28]S. C. Stacy and M. L. Pantoya, "Laser ignition of nano-composite energetic loose powders," Prop. Explos. Pyrotech. **38**, 441–447 (2013).
[29]E. M. Hunt and M. L. Pantoya, "Ignition dynamics and activation energies of metallic thermites: From nano- to micron-scale particulate composites," J. Appl. Phys. **98** 034909 (2005).
[30]K. C. Walter, C. E. Aumann, R. D. Carpenter, E. H. O'Neill, and D. R. Pesiri, "Energetic materials development at technanogy materials development," MRS Proc. **800**, AA1.3 (2003).
[31]Y. Ohkura, P. M. Rao, and X. Zheng, "Flash ignition of Al nanoparticles: Mechanism and applications," Combust. Flame **158**, 2544–2548 (2011).
[32]M. R. Weismiller, J. Y. Malchi, R. A. Yetter, and T. J. Foley, "Dependence of flame propagation on pressure and pressurizing gas for an Al/CuO nanoscale thermite," Proc. Combust. Inst. **32 II**, 1895–1903 (2009).
[33]T. W. Barbee, Jr., A. E. Gash, J. H. Satcher, Jr., and R. L. Simpson, *Nanotechnology Based Environmentally Robust Primers* (Lawrence Livermore National Lab., Livermore, CA, 2003).
[34]J. J. Granier and M. L. Pantoya, "Laser ignition of nanocomposite thermites," Combust. Flame **138**, 373–383 (2004).
[35]L. De Yong, T. Nguyen, and J. Waschl, *Laser Ignition of Explosives, Pyrotechnics and Propellants: A Review* (Defence Science and Technology Organization, Canberra, Australia, 1995).
[36]M. Petrantoni, C. Rossi, V. Conédéra, D. Bourrier, P. Alphonse, and C. Tenailleau, "Synthesis process of nanowired Al/CuO thermite," J. Phys. Chem. Solids **71**, 80–83 (2010).